Nuclear Engineering and Technology 54 (2022) 3440–3447

Contents lists available at ScienceDirect

Nuclear Engineering and Technology

journal homepage: www.elsevier.com/locate/net

Original Article

Effect of the new photoatomic data library EPDL2017 to mass attenuation coefficient calculation of materials used in the nuclear medicine facilities using EpiXS software

J.F.M. Jecong*, F.C. Hila, C.V. Balderas, N.R.D. Guillermo

Department of Science and Technology - Philippine Nuclear Research Institute (DOST-PNRI), Commonwealth Avenue, Diliman, Quezon City, 1101, Philippines

ARTICLE INFO

Article history:
Received 15 April 2021
Received in revised form
20 March 2022
Accepted 22 March 2022
Available online 29 March 2022

Keywords:
EPDL2017 library
Mass attenuation coefficient
X-ray
Gamma-ray
Radiation shielding
Nuclear medicine

ABSTRACT

The accuracy of the photoatomic cross-section data is of great importance in the field of radiation protection, particularly in the characterization of radiation shielding materials. With the release of the latest and probably the most accurate photoatomic data library, EPDL2017, the need to re-evaluate all the existing and already established mass attenuation coefficients (MACs) of all radiation shielding materials arises. The MACs of several polymers, alloy-based, glasses, and building materials used in a nuclear medicine facility were investigated using the EPDL2017 library embedded in EpiXS software and were compared to MACs available in the literature. The relative differences between MAC_{EpiXS} and MAC_{XCOM} were negligible, ranging from 0.02% to 0.36% for most materials. However, for material like a glass comprising of elements Te and La evaluated near their corresponding K-edge energies, the relative differences in MACs increased up to 1.46%. On the other hand, a comparison with MACs calculated based on EPDL97 (a predecessor of EPDL2017) revealed as much as a 6.61% difference. Also, it would seem that the changes in MACs were more evident in the materials composed of high atomic number elements evaluated at x-ray energies compared to materials composed of low atomic number elements evaluated at gamma-ray energies.

1. Introduction

For the past half-century, nuclear medicine is continuously evolving as multidisciplinary sciences advance, new techniques are developed, and new technologies emerge. Due to the numerous beneficial uses of radiation, the number of radionuclides being studied and utilized in medicine continues to increase. It was estimated by the International Atomic Energy Agency (IAEA) that the number of nuclear medicine examinations worldwide in 2014 is averaging by 35 million per year. This makes medical exposure the leading human-made source of radiation exposure [1].

Depending on the type of exam, nuclear medicine can be an arduous procedure that requires prolonged and continuous exposure of the patient to ionizing radiation. Whether for diagnosis, evaluation, or therapy of diseases, nuclear medicine procedures can be time-consuming. Radiotracers could take several hours to days to travel through the body and accumulate in the area of interest while it can take several hours to perform imaging. Moreover, nuclear medicine also involves exposure to the medical physicist, nuclear medicine physicians, technologists, carers and comforters of patients undergoing procedures, and members of the public [2,3].

No matter how small, exposure carries risks of unwanted health and environmental effects, especially for continuous exposure [4]. To ensure that the occurrence of deterministic effects is prevented, the probability of stochastic effects is minimized to an acceptable level, and the damage to the nearby environment is avoided, materials possessing excellent radiation shielding properties are of great importance in nuclear medicine. The efficacy of such materials in shielding radiation at various energies is usually gauged by their mass attenuation coefficients (MACs). MAC is a constant that describes the fraction of radiations reduced per unit mass from a radiation beam by an absorber or material. It is used to quantify radiation penetration and energy deposition in shielding and other dosimetric materials. Thereby, the MACs of countless polymers [5–7], alloys [6,8,9], ceramics [10,11], glasses [12–14], concretes [15–17], and other materials [4,18,19] have been determined to assess their radiation shielding capabilities.

* Corresponding author.
E-mail address: jmjecong@pnri.dost.gov.ph (J.F.M. Jecong).

https://doi.org/10.1016/j.net.2022.03.030

The MAC can be obtained through an experiment and calculations using simulation programs. The experiment is conducted by measuring the narrow x-ray and gamma-ray transmission to the material [13,20–23]. However, this method is associated with handling x-ray equipment and radioactive sources, which requires adherence to the radiation safety protocols. Due to the steep requirements, relatively few research studies on radiation shielding have been conducted experimentally. On the other hand, the most common way of obtaining MAC is via computer programs such as XCOM, WinXCom, MCNP, Geant4, and PENELOPE [14,24–28]. Although calculations using computer programs have the advantage of investigating the radiation shielding capabilities of the material without the risks of radiation exposure, the accuracy is highly dependent on their photoatomic data library. On this matter, it should be emphasized that the EPDL97, the data library of Monte Carlo-based simulation codes (MCNP5, Geant4, PENELOPE, etc.) was developed in 1997, while the NIST-XCOM library, the data library of most photon attenuation software (XCOM, WinXCom, Phy-X/PSD, etc) was last updated in 2010. With the advancement of science and technology, the study of past experiments, and analyses of previous data stimulate the improvements, in theory, simulations, and experiments that give birth to more precise data. Presumably, a new photoatomic data library has more accurate atomic information than the old data libraries.

In 2017, the International Atomic Energy Agency Nuclear Data Services (IAEA-NDS) released the most up-to-date and official ENDF/B-VIII electron and photon data library, EPICS2017 [29] to replace all earlier versions of EPICS data libraries. Among the three sub-libraries of EPICS2017, new photoatomic data can be found in the Evaluated Photon Data Library (EPDL2017). In this new data sub-library, the subshell binding energies have been adjusted that resulted in an improved photoelectric cross-section, anomalous scattering factors, and coherent scatter [30]. Research has already been conducted that uses the EPDL2017 library in radiation shielding parameters calculation and the results were compared with the experimental data, Monte Carlo-based simulation codes, and photon attenuation software [31–35]. However, these researches involved extraction and interpolation of EPICS2017 library for calculation which is a complicated process. Furthermore, although the initial assessment shows MACs evaluated with EPDL2017 are in good agreement with MACs derived from other methods, this is only true for a limited number of materials and energies involved in those studies.

Recently, windows-based application software for photon attenuation based on EPDL2017 of ENDF/B-VIII and EPDL97 of ENDF/B-VI.8 photoatomic data library was developed [36]. In this study, the EpiXS software was used in calculating the MAC (MAC_{EpiXS}) at x-ray and gamma-ray energies. The results were compared with the MACs evaluated with the old photon data libraries from literature to give more information on how the new photoatomic data library may affect the MACs calculations of several multi-element materials commonly employed in nuclear medicine facilities.

Table 1
The elemental compositions of several materials used in nuclear medicine facilities.

	Elemental Composition (wt%)
Polymers[a]	
Polyetherimide	H (4.08), C (74.99), N (4.73), O (16.20)
Polysulfone	H (5.01), C (73.28), O (14.46), S (7.25)
Polyether ketone	H (7.43), C (76.48), O (16.09)
Poly (ether sulfone)	H (3.47), C (62.06), O (20.67), S (13.81)
Poly (butylene terephthalate)	H (5.49), C (65.45), O (29.06)
Poly (ethylene isophthalate)	H (4.20), C (62.50), O (33.30)
Poly (butyl methacrylate)	H (9.92), C (67.57), O (22.50)
Poly (phenylene oxide)	H (6.71), C (79.97), O (13.32)
Polymethyl pentane	H (14.37), C (85.63)
High-density Polyethylene	H (14.37), C (85.63)
Alloy-based[b,c]	
FeCr(5%)	Co (0.03), C (57.21), H (4.38), O (33.78), Fe (2.38), Cr (2.22)
FeCr(10%)	Co (0.03), C (54.69), H (4.18), O (32.29), Fe (4.56), Cr (4.24)
FeCr(15%)	Co (0.03), C (52.38), H (4.01), O (30.93), Fe (6.55), Cr (6.10)
Tungsten Carbide	W (98.65), C (1.35)
Glasses[d]	
A	Te (51.87), B (3.77), Zn (16.27), La (2.33), O (25.76)
B	Te (50.47), B (3.67), Zn (15.83), La (4.58), O (25.46)
C	Te (49.11), B (3.57), Zn (15.41), La (6.75), O (25.17)
D	Te (47.80), B (3.47), Zn (14.99), La (8.85), O (24.89)
E	Te (46.53), B (3.38), Zn (14.60), La (10.88), O (24.62)
Rocks/Concrete[e]	
Feldspathic basalt	O (44.35), Na (2.92), Mg (2.40), Al (6.71), Si (23.94), P (0.17), K (0.77), Ca (7.87), Ti (1.41), Mn (0.13), Fe (9.32)
Compact basalt	O (44.54), Na (3.28), Mg (2.06), Al (6.33), Si (24.50), P (0.24), K (0.83), Ca (6.44), Ti (1.70), Mn (0.13), Fe (9.96)
Volcanic rock	O (43.43), Na (3.89), Mg (2.46), Al (6.15), Si (22.21), P (0.37), K (1.17), Ca (8.66), Ti (2.17), Mn (0.21), Fe (9.30)
Pink granite	O (48.76), Na (3.83), Mg (<0.01), Al (5.5), Si (35.83), P (0.02), K (4.10), Ca (0.50), Ti (0.10), Mn (0.02), Fe (1.32)
Sandstone	O (52.67), Na (0.01), Mg (<0.00), Al (2.81), Si (43.70), P (0.02), K (<0.00), Ca (0.22), Ti (0.07), Mn (0.01), Fe (0.49)
Dolerite	O (44.00), Na (2.98), Mg (2.29), Al (6.47), Si (22.98), P (0.15), K (0.26), Ca (7.08), Ti (2.25), Mn (0.17), Fe (11.39)
Concrete	O (45.56), Na (4.18), Mg (2.97), Al (4.18), Si (12.21), K (1.93), Ca (24.96), Ti (0.02), Fe (1.60), S (0.22), H (0.87), C (2.56)

[a] More et al. [20].
[b] Akman et al. [38].
[c] AbuAlRoos et al. [37].
[d] Lakshminarayana et al. [24].
[e] Obaid et al. [39].

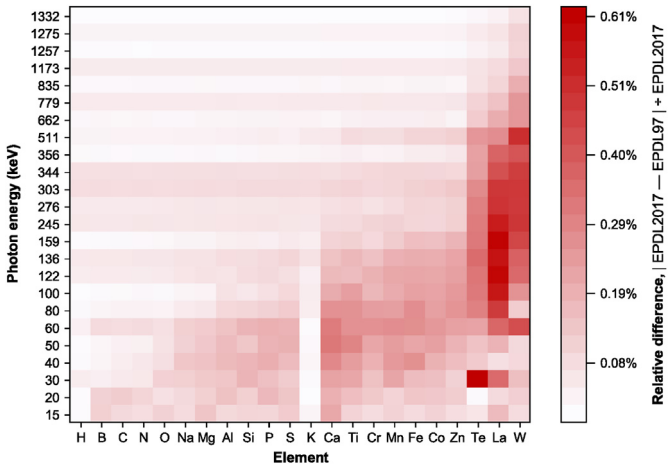

Fig. 1. Comparison of cross-sections from ENDF/B-VIII (EPDL2017) and the ENDF/B-VI.8 (EPDL97).

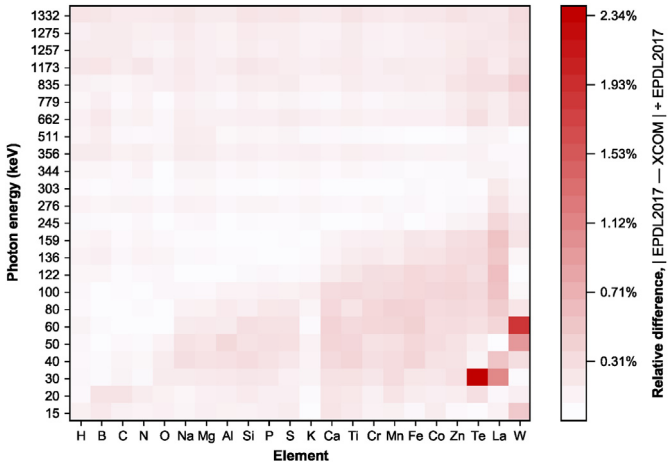

Fig. 2. Comparison of cross-sections from ENDF/B-VIII (EPDL2017) and the XCOM.

2. Materials and method

2.1. Materials used in nuclear medicine facilities

Ten thermoplastic polymers [20], a lead-free tungsten carbide material [37], three FeCr doped polyester composites alloy [38], five lead-free TeO_2–B_2O_3–ZnO–La_2O_3 glasses [24], and seven types of concrete and rocks [39] employed in nuclear medicine facilities were used in this study. The MACs of these materials were evaluated using the EpiXS software's EPDL2017 library at x-ray (15–100 keV) and gamma-ray (122–1332 keV) energies. These materials were chosen because their ionizing radiation shielding properties had already been determined using an experiment (narrow beam transmission setup), photon attenuation software (XCOM, WinXCom), and Monte Carlo-based simulation codes (MCNP, Geant4, PENELOPE). The elemental compositions of the materials of interest are presented in Table 1.

2.2. EpiXS software

EpiXS is a new software with embedded EPDL2017 of ENDF/B-VIII and EPDL97 of ENDF/B-VI.8 libraries designed for shielding, dosimetry, and photon attenuation calculations. This software can provide the MAC (partials, total), as well as other fundamental photon attenuation parameters including cross-sections (partials, total, electronic), linear attenuation coefficients (partials, total), mean free paths, half-value layers, effective atomic numbers (direct, interpolation), effective electron densities (direct, interpolation), ratios of Compton cross-sections to total cross-sections (no coherent), equivalent atomic numbers, G-P fitting parameters (exposure or energy absorption), and buildup factors (exposure or energy absorption) at any specific energies between 1 keV and 100 GeV. EpXS employs the interpolation principles specified by each photoatomic library. Moreover, it has a simple interface and allows for quick interactive graphing and data tabulations, making it an excellent tool for comparing and extracting data from data libraries. Because of its efficient set of algorithms, any photon parameters for a material entry spanning all 100 elements in a broad energy grid can be generated in less than 1 s for a material entry covering all 100 elements in a broad energy grid. Additionally, EpiXS can display X-ray absorption edge energies using EPICS2017 or EPDL97.

The total MAC or $(\frac{\mu}{\rho})$ is expressed as

$$(\frac{\mu}{\rho})_T = \sigma_T \frac{N_A}{\sum f_i A_i}, \quad (1)$$

where N_A is Avogadro's number, f_i and A_i are the corresponding atom fraction and atomic mass of the ith element, and σ_T is the total atomic cross-section. σ_T is calculated by summing up the partial cross-sections of photoelectric (σ_{PE}), coherent (σ_{coh}), incoherent (σ_{incoh}), pair production in the nuclear field (σ_{PP-N}), and pair production in electron field (σ_{PP-E}).

$$\sigma_T = \sigma_{PE} + \sigma_{coh} + \sigma_{incoh} + \sigma_{PP-N} + \sigma_{PP-E} \quad (2)$$

3. Results and discussion

The σ_T is directly proportional to the MAC which means that any changes in the σ_T will affect the calculation of MAC. Thus, evaluating the EPDL2017 and determining its difference from EPDL97 and XCOM libraries will give insights into how the already established MACs of several multi-element materials in the literature be altered for using the most up-to-date atomic data library.

The EPDL2017 photoatomic cross-sections of all the material's elemental composition included in this study are mapped and compared with EPDL and XCOM at various x-ray and gamma-ray

Table 2
Comparison of K-edge energies and the corresponding photoelectric cross-sections.

Element	EPDL2017		EPDL97		XCOM	
	K-edge (keV)	cross-section (barns/atom)	K-edge (keV)	cross-section (barns/atom)	K-edge (keV)	cross-section (barns/atom)
Te	31.82	7724	31.81	7733	31.81	7723
La	38.93	6203	38.94	6198	38.92	6245
W	69.53	3285	69.69	3262	69.53	3297

Table 3
Comparison of MAC_{EpiXS} (cm^2/g) from MAC_{exp}, $MAC_{WinXCom}$, and MAC_{MCNPX} – polymers [20].

Polymers	122 keV				356 keV				511 keV				662 keV			
	EpiXS	Exp.	WinXCom	MCNPX	EpiXS	Exp.	WinXCom	MCNPX	EpiXS	Exp.	WinXCom	MCNPX	EpiXS	Exp.	WinXCom	MCNPX
PEA	0.1491	0.1482	0.1491	0.1483	0.1039	0.1021	0.1040	0.1036	0.0898	0.0875	0.0899	0.0898	0.0802	0.0789	0.0803	0.0799
PSU	0.1523	0.1492	0.1524	0.1480	0.1049	0.1025	0.1050	0.1021	0.0906	0.0893	0.0907	0.0886	0.0809	0.0791	0.0810	0.0788
PEK	0.1536	0.1502	0.1537	0.1521	0.1071	0.1032	0.1073	0.1058	0.0926	0.0919	0.0927	0.0923	0.0828	0.0811	0.0828	0.0825
PES	0.1522	0.1501	0.1523	0.1523	0.1035	0.1002	0.1036	0.1024	0.0894	0.0845	0.0894	0.0865	0.0798	0.0761	0.0799	0.0772
PBT	0.1513	0.1486	0.1513	0.1511	0.1053	0.1012	0.1054	0.1028	0.0910	0.0901	0.0911	0.0910	0.0813	0.0794	0.0814	0.0803
PEI	0.1496	0.1465	0.1497	0.1490	0.1040	0.1027	0.1041	0.1038	0.0899	0.0879	0.0899	0.0899	0.0803	0.0787	0.0804	0.0801
PBMA	0.1572	0.1527	0.1573	0.1548	0.1096	0.1069	0.1097	0.1091	0.0947	0.0918	0.0948	0.0935	0.0847	0.0819	0.0847	0.0844
PPO	0.1526	0.1493	0.1526	0.1524	0.1064	0.1043	0.1066	0.1060	0.0920	0.0904	0.0921	0.0918	0.0822	0.0801	0.0823	0.0817
PMP	0.1628	0.1601	0.1629	0.1621	0.1139	0.1119	0.1140	0.1134	0.0985	0.0956	0.0986	0.0982	0.0880	0.0862	0.0881	0.0881
HDPE	0.1628	0.1605	0.1629	0.1627	0.1139	0.1122	0.1140	0.1139	0.0985	0.0954	0.0986	0.0977	0.0880	0.0866	0.0881	0.0880
Polymers	835 keV				1173 keV				1257 keV				1332 keV			
	EpiXS	Exp.	WinXCom	MCNPX	EpiXS	Exp.	WinXCom	MCNPX	EpiXS	Exp.	WinXCom	MCNPX	EpiXS	Exp.	WinXCom	MCNPX
PEA	0.0721	0.0702	0.0720	0.0713	0.0610	0.0599	0.0612	0.0607	0.0585	0.0569	0.0586	0.0581	0.0572	0.0558	0.0573	0.0569
PSU	0.0727	0.0711	0.0726	0.0704	0.0616	0.0596	0.0618	0.0599	0.0591	0.0572	0.0591	0.0573	0.0577	0.0551	0.0579	0.0560
PEK	0.0744	0.0721	0.0742	0.0734	0.0630	0.0618	0.0632	0.0626	0.0604	0.0591	0.0605	0.0603	0.0590	0.0576	0.0592	0.0586
PES	0.0717	0.0701	0.0716	0.0711	0.0607	0.0575	0.0609	0.0590	0.0582	0.0568	0.0583	0.0581	0.0569	0.0549	0.0570	0.0561
PBT	0.0731	0.0714	0.0729	0.0727	0.0619	0.0601	0.0621	0.0617	0.0593	0.0576	0.0594	0.0582	0.0580	0.0561	0.0581	0.0576
PEI	0.0722	0.0709	0.0721	0.0720	0.0611	0.0592	0.0613	0.0611	0.0586	0.0559	0.0587	0.0572	0.0573	0.0557	0.0574	0.0568
PBMA	0.0761	0.0732	0.0759	0.0740	0.0644	0.0623	0.0646	0.0636	0.0618	0.0603	0.0618	0.0618	0.0603	0.0591	0.0605	0.0601
PPO	0.0739	0.0724	0.0737	0.0737	0.0626	0.0604	0.0628	0.0618	0.0600	0.0589	0.0601	0.0600	0.0586	0.0545	0.0588	0.0561
PMP	0.0791	0.0763	0.0789	0.0775	0.0670	0.0651	0.0672	0.0671	0.0642	0.0617	0.0643	0.0631	0.0627	0.0604	0.0629	0.0615
HDPE	0.0791	0.0765	0.0789	0.0781	0.0670	0.0659	0.0672	0.0671	0.0642	0.0621	0.0643	0.0631	0.0627	0.0613	0.0629	0.0626

Table 4
Comparison of MAC_{EpiXS} (cm^2/g) from MAC_{exp}, MAC_{XCOM}, and MAC_{MCNPX} – alloy-based [37,38].

Alloy-based	60 keV				81 keV				122 keV				136 keV			
	EpiXS	Exp.	XCOM	MCNPX	EpiXS	Exp.	XCOM	MCNPX	EpiXS	Exp.	XCOM	MCNPX	EpiXS	Exp.	XCOM	MCNPX
FeCr(5%)	0.2314	0.2207	0.2311	0.2336	0.1864	0.1812	0.1863	0.1823	0.1547	0.1514	0.1547	0.1526	0.1483	0.1556	0.1483	0.1574
FeCr(10%)	0.2704	0.2631	0.2699	0.2712	0.2016	0.2102	0.2015	0.2058	0.1588	0.1540	0.1588	0.1592	0.1510	0.1581	0.1511	0.1533
FeCr(15%)	0.3060	0.3068	0.3051	0.3142	0.2155	0.2059	0.2152	0.2173	0.1625	0.1603	0.1625	0.1634	0.1536	0.1517	0.1536	0.1539
Tungsten Carbide	–	–	–	–	–	–	–	–	–	–	–	–	–	–	–	–
Alloy-based	159 keV				245 keV				276 keV				303 keV			
	EpiXS	Exp.	XCOM	MCNPX	EpiXS	Exp.	XCOM	MCNPX	EpiXS	Exp.	XCOM	MCNPX	EpiXS	Exp.	XCOM	MCNPX
FeCr(5%)	–	–	–	–	–	–	–	–	0.1148	0.1124	0.1149	0.1142	0.1110	0.1060	0.1110	0.1122
FeCr(10%)	–	–	–	–	–	–	–	–	0.1148	0.1136	0.1149	0.1159	0.1108	0.1061	0.1109	0.1114
FeCr(15%)	–	–	–	–	–	–	–	–	0.1147	0.1114	0.1148	0.1151	0.1107	0.1154	0.1107	0.1111
Tungsten Carbide	1.354	1.207	1.351	–	0.491	0.469	0.491	–	–	–	–	–	–	–	–	–
Alloy-based	344 keV				356 keV				662 keV				779 keV			
	EpiXS	Exp.	XCOM	MCNPX	EpiXS	Exp.	XCOM	MCNPX	EpiXS	Exp.	XCOM	MCNPX	EpiXS	Exp.	XCOM	MCNPX
FeCr(5%)	–	–	–	–	–	–	–	–	–	–	–	–	–	–	–	–
FeCr(10%)	–	–	–	–	–	–	–	–	–	–	–	–	–	–	–	–
FeCr(15%)	–	–	–	–	–	–	–	–	–	–	–	–	–	–	–	–
Tungsten Carbide	0.247	0.239	0.247	–	0.233	0.209	0.233	–	0.097	0.09	0.098	–	0.082	0.077	0.083	–

Table 5
Comparison of MAC_{EpiXS} (cm^2/g) from MAC_{exp}, MAC_{XCOM}, and MAC_{MCNPX} - glass [24].

Glass	15 keV					20 keV					30 keV				
	EpiXS	WinXCom	MCNP5	Geant4	Penelope	EpiXS	WinXCom	MCNP5	Geant4	Penelope	EpiXS	WinXCom	MCNP5	Geant4	Penelope
A	41.6169	41.6090	41.6013	41.5940	41.0156	19.1316	19.1580	19.1402	19.1250	18.8761	6.3092	6.4010	6.3329	6.3320	6.2568
B	42.0540	42.0440	42.0339	42.0290	41.4355	19.3368	19.3630	19.3472	19.3300	19.0743	6.3803	6.4721	6.4047	6.4033	6.3262
C	42.4764	42.4650	42.4440	42.4500	41.8388	19.5351	19.5610	19.5387	19.5280	19.2646	6.4490	6.5409	6.4723	6.4722	6.3928
D	42.8846	42.8710	42.8482	42.8560	42.2318	19.7268	19.7520	19.7288	19.7190	19.4500	6.5153	6.6075	6.5404	6.5389	6.4576
E	43.2796	43.2650	43.2432	43.2490	42.6119	19.9122	19.9370	19.9104	19.9040	19.6294	6.5796	6.6719	6.6050	6.6033	6.5203
Glass	40 keV					50 keV					60 keV				
	EpiXS	WinXCom	MCNP5	Geant4	Penelope	EpiXS	WinXCom	MCNP5	Geant4	Penelope	EpiXS	WinXCom	MCNP5	Geant4	Penelope
A	12.2505	12.2600	12.2382	12.2360	12.1743	6.8181	6.8080	6.8077	6.8080	6.7746	4.2143	4.2020	4.2036	4.2054	4.1826
B	12.5124	12.5250	12.5021	12.4990	12.4347	6.9686	6.9591	6.9570	6.9582	6.9239	4.3087	4.2963	4.2977	4.2993	4.2760
C	12.7655	12.7800	12.7526	12.7530	12.6833	7.1140	7.1048	7.1053	7.1033	7.0665	4.3999	4.3870	4.3903	4.3900	4.3651
D	13.0101	13.0280	12.9995	12.9980	12.9269	7.2546	7.2456	7.2450	7.2436	7.2062	4.4881	4.4748	4.4770	4.4777	4.4524
E	13.2468	13.2670	13.2354	13.2360	13.1645	7.3906	7.3819	7.3789	7.3793	7.3423	4.5734	4.5597	4.5625	4.5626	4.5375

Glass	80 keV					100 keV				
	EpiXS	WinXCom	MCNP5	Geant4	Penelope	EpiXS	WinXCom	MCNP5	Geant4	Penelope
A	1.9768	1.9710	1.9651	1.9709	1.9624	1.1179	1.1140	1.1106	1.1144	1.1098
B	2.0209	2.0144	2.0098	2.0146	2.0060	1.1420	1.1382	1.1358	1.1383	1.1336
C	2.0634	2.0567	2.0527	2.0569	2.0477	1.1653	1.1613	1.1590	1.1614	1.1563
D	2.1046	2.0976	2.0950	2.0978	2.0884	1.1878	1.1836	1.1811	1.1837	1.1786
E	2.1444	2.1372	2.1348	2.1374	2.1281	1.2096	1.2053	1.2027	1.2053	1.2003

Table 6
Comparison of MAC_{EpiXS} (cm^2/g) from MAC_{exp}, MAC_{XCOM}, and MAC_{MCNPX} – construction/rocks [39].

Construction/Rocks	122 keV			356 keV			511 keV		
	EpiXS	Exp.	XCOM	EpiXS	Exp.	XCOM	EpiXS	Exp.	XCOM
Feldspathic basalt	0.167	0.182	0.167	0.100	0.101	0.100	0.086	0.087	0.086
Compact basalt	0.167	0.181	0.167	0.100	0.098	0.100	0.086	0.087	0.086
Volcanic rock	0.167	0.180	0.167	0.100	0.110	0.100	0.086	0.089	0.086
Pink granite	0.155	0.167	0.155	0.100	0.110	0.100	0.086	0.089	0.086
Sandstone	0.153	0.151	0.153	0.100	0.099	0.100	0.086	0.086	0.086
Dolerite	0.169	0.175	0.169	0.100	0.099	0.100	0.086	0.084	0.086
Concrete	0.166	0.154	0.166	0.101	0.102	0.102	0.087	0.087	0.087
Construction/Rocks	662 keV			1170 keV			1275 keV		
	EpiXS	Exp.	XCOM	EpiXS	Exp.	XCOM	EpiXS	Exp.	XCOM
Feldspathic basalt	0.077	0.078	0.077	0.058	0.059	0.058	0.056	0.056	0.056
Compact basalt	0.076	0.078	0.077	0.058	0.059	0.058	0.056	0.057	0.056
Volcanic rock	0.076	0.080	0.077	0.058	0.059	0.058	0.056	0.056	0.056
Pink granite	0.077	0.080	0.077	0.058	0.06	0.058	0.056	0.057	0.056
Sandstone	0.077	0.077	0.077	0.059	0.056	0.059	0.056	0.054	0.056
Dolerite	0.076	0.077	0.076	0.058	0.056	0.058	0.056	0.055	0.056
Concrete	0.078	0.078	0.078	0.059	0.058	0.059	0.057	0.057	0.057

Construction/Rocks	1330 keV		
	EpiXS	Exp.	XCOM
Feldspathic basalt	0.055	0.056	0.055
Compact basalt	0.055	0.056	0.055
Volcanic rock	0.055	0.056	0.055
Pink granite	0.055	0.056	0.056
Sandstone	0.056	0.053	0.056
Dolerite	0.055	0.054	0.055
Concrete	0.056	0.055	0.056

Figs. 1 and 2. The cross-section data of EPDL2017 and EPDL97 were obtained using the EpiXS software. In both figures, the elements are arranged in increasing atomic numbers from left to right. The differences between the two versions of the EPDL libraries are noticeable at lower energies where the photoelectric effect is dominant as shown in Fig. 1. Furthermore, the differences are relatively higher (~0.6%) for elements Te, La, and W at energies near their corresponding K-edge energies. These findings are expected because the subshell binding energies have been modified in EPDL2017, which in turn improved the photoelectric cross-sections. Noticeably, similar to Fig. 1, the differences between EPDL2017 and XCOM are also quite apparent (~2.3%) for elements Te, La, and W at energies near their corresponding K-edge energies (see Fig. 2). Table 2 shows the differences in the K-edge energies and the corresponding cross-sections of the elements Te, La, and W from three data libraries.

Comparisons of MAC_{EpiXS} and MAC evaluated from experiments (MAC_{Exp}), XCOM (MAC_{XCOM}), WinXCom ($MAC_{WinXCom}$), MCNP (MAC_{MCNP}), Geant4 (MAC_{Geant4}), and PENELOPE ($MAC_{PENELOPE}$) of different multi-element materials used in nuclear medicines

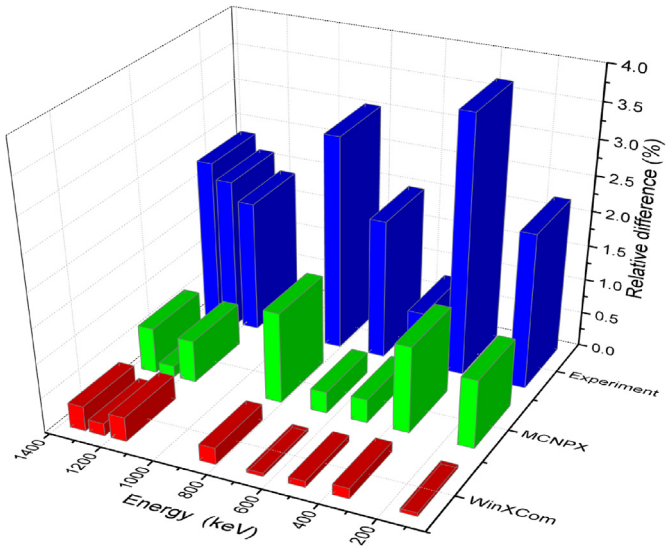

Fig. 3. Comparison of MAC_{EpiXS} from MAC_{exp}, $MAC_{WinXCom}$, and MAC_{MCNPX} - Polyether ketone [20].

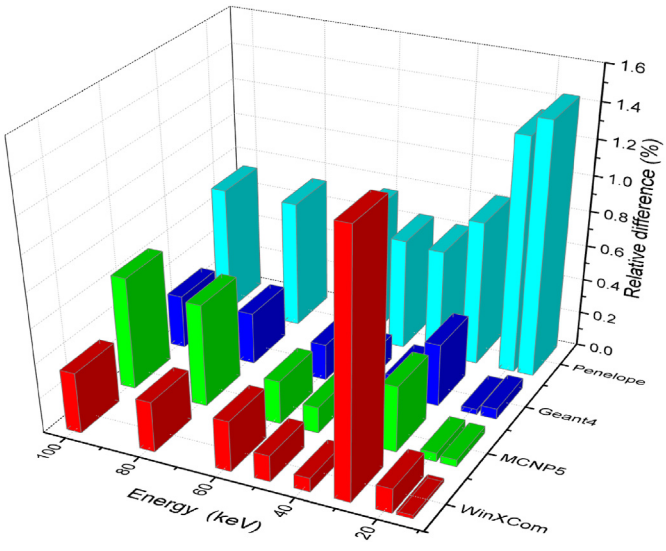

Fig. 5. Comparison of MAC_{EpiXS} from $MAC_{WinXCom}$, MAC_{MCNP5}, MAC_{Geant4}, and $MAC_{Penelope}$ – glass A [24].

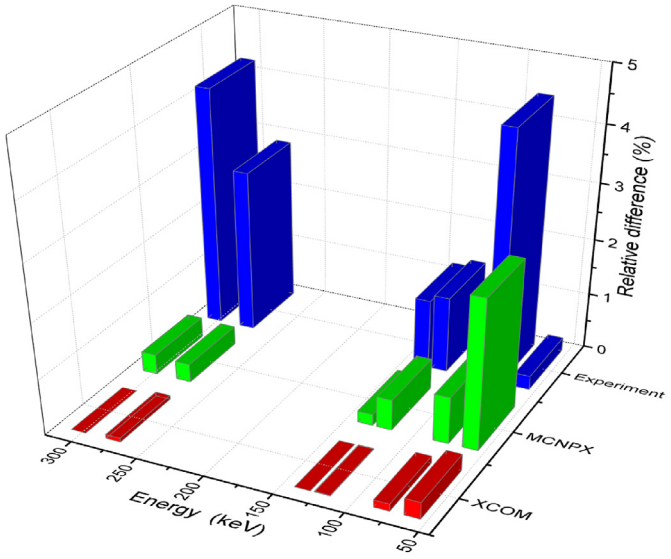

Fig. 4. Comparison of MAC_{EpiXS} from MAC_{exp}, MAC_{XCOM}, and MAC_{MCNPX} - alloy-based FeCr(15%) [37,38].

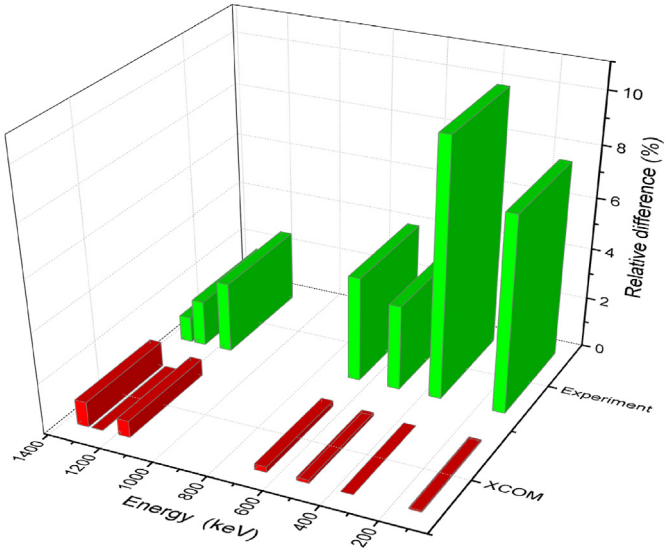

Fig. 6. Comparison of MAC_{EpiXS} from $MAC_{WinXCom}$ and MAC_{Exp} – pink granite [39].

facilities are summarized in Tables 3–6. These materials under review include ten polymers comprising of H, C, N, O, and S; four alloy-based comprising of Co, C, H, O, Fe, Cr, and W; five glasses comprising of Te, B, Zn, La, O, and seven construction building materials comprising of O, Na, Mg, Al, Si, P, K, Ca, Ti, Mn, Fe, S, H, and C. Additionally, the changes in MAC calculations using EPDL2017 for polyether ketone (polymers), FeCr-15% (alloy-based), Glass A, and pink granite (rocks) are highlighted in Figs. 3–6.

In most materials under investigation, the relative difference between MAC_{EpiXS} and MAC_{XCOM} is negligible, ranging from 0.02% to 0.36%. The same assessment is also true between MAC_{EpiXS} and $MAC_{WinXCom}$ since the WinXCom software is based on the XCOM library. However, it is not true for the material comprising elements Te, La, or W evaluated near their corresponding K-edge energies. A good example is the material Glass A in which a relative difference of 1.46% is measured between MAC_{EpiXS} and $MAC_{WinXCom}$ evaluated at 30 keV as shown in Fig. 5. More than 50% of this glass is composed of elements Te and La contributing to the relatively higher differences in the calculated MACs. Another example of the material with element W under examination is the tungsten carbide in Table 4. It was evaluated at energies far from its K-edge energy, thus the difference in MAC calculation is not noticeable.

In the case of Glass samples, the relative difference of MAC_{EpiXS} to other Monte Carlo-based simulation codes ($MAC_{MCNP,}$ MAC_{Geant4}, and $MAC_{PENELOPE}$) is as much as 6.61%. As discussed earlier, the relatively high difference mainly comes from the noticeable changes in glass samples composition Te and La cross-sections in the EPDL2019 library (see Fig. 1), and the energies wherein MAC was evaluated (near their K-edge energies). Notably, with a similar experimental setup, material, and photoatomic library, the MAC_{MCNP} should be equal to MAC_{Geant4} and $MAC_{PENELOPE}$. The differences in their calculation mainly come from how the boundary conditions (geometry) of the experimental setup were defined in each code.

On the other hand, the highest difference can be seen between

MAC_{EpiXS} and MAC_{Exp}, emphasized in Figs. 3, 4 and 6. The MAC equation was derived from an assumption of narrow beam geometry, mono-energetic photons, and a thin absorbing material. However, these assumptions are difficult to achieve in an experiment, thus deviation from theoretical MAC is inevitable. The closer the experiment to these assumptions, the lesser the relative difference between the two methods. Furthermore, uncertainties in peak area analysis, counting statistics, and uncertainties in material thickness and density may further increase the relative difference. It is worth noting the MAC_{Exp} is closer to MAC_{EpiXS} than to MAC evaluated using other aforementioned methods suggesting that the EPDL2017 library having the most precise photoatomic cross-sections among other photoatomic data libraries.

4. Conclusion

The MACs of several multi-element polymers, alloy-based, glasses, and building materials that can be found in nuclear medicine facilities were evaluated from x-ray to gamma-ray energies using the EPDL2017 library of EpiXS software. The relative difference between MAC_{EpiXS} and other photon attenuation software (MAC_{XCOM} and $MAC_{WinXCom}$) is negligible in most materials under investigation, ranging from 0.02% to 0.36%. On the other hand, the relative difference between MAC_{EpiXS} and the other Monte Carlo-based simulation codes (MAC_{MCNP}, MAC_{Geant4}, and $MAC_{PENELOPE}$) is as much as 6.61%, which is due primarily to how the boundary conditions of the experimental setup were defined in each code. Noticeable changes in MACs are observed when evaluated at x-ray energies (1 keV–100 keV) especially near the comprising elements K-edge energies of the materials. Moreover, the changes in MACs are relatively higher for materials consisting of elements Te, La, or W. Comparison with the experimental MACs implies that EPDL2017 is better than other libraries in terms of photoatomic data accuracy.

The EpiXS software is user-friendly, easy to navigate, aesthetically appealing, has a well-designed graphical user interface, fast and accurate, and easy to acquire software. Like other theoretical software and Monte Carlo-based simulation codes, EpiXS could allow anyone, including those with no access to photon energies in the keV to GeV range to research the ionizing shielding capabilities of any materials with the most up-to-date and presumably most accurate photoatomic library.

Declaration of competing interest

The authors declare that they have no known competing financial interests or personal relationships that could have appeared to influence the work reported in this paper.

References

[1] D.L. Bailey, J.L. Humm, A. Todd-Pokropek, A. van Aswegen, Nuclear Medicine Physics: A Handbook for Teachers and Students, 2014.

[2] M. Marengo, C.J. Martin, S. Rubow, T. Sera, Z. Amador, L. Torres, Radiation safety and accidental radiation exposures in nuclear medicine, Semin. Nucl. Med. 52 (2) (2021) 94–113, https://doi.org/10.1053/j.semnuclmed.2021.11.006.

[3] T. Portela, T.S.C. Camozzato, R. de C. Flôr, G. Ribeiro, J.A.C. de Melo, Occupational exposure in the working process of radiological nursing in nuclear medicine, J. Radiol. Nurs. 40 (3) (2021) 246–253, https://doi.org/10.1016/j.jradnu.2021.02.005.

[4] D. Adliene, L. Gilys, E. Griskonis, Development and characterization of new tungsten and tantalum containing composites for radiation shielding in medicine, Nucl. Instrum. Methods Phys. Res. B 467 (2020) 21–26.

[5] F. Akman, M.R. Kaçal, N. Almousa, M.I. Sayyed, H. Polat, Gamma-ray attenuation parameters for polymer composites reinforced with BaTiO3 and CaWO4 compounds, Prog. Nucl. Energy 121 (2020), https://doi.org/10.1016/j.pnucene.2020.103257. December 2019.

[6] F. Akman, M.R. Kaçal, M.I. Sayyed, H.A. Karataş, Study of gamma radiation attenuation properties of some selected ternary alloys, J. Alloys Compd. 782 (2019) 315–322, https://doi.org/10.1016/j.jallcom.2018.12.221.

[7] M.R. Kaçal, F. Akman, M.I. Sayyed, Evaluation of gamma-ray and neutron attenuation properties of some polymers, Nucl. Eng. Technol. 51 (3) (2019) 818–824, https://doi.org/10.1016/j.net.2018.11.011.

[8] F. Akman, M.I. Sayyed, M.R. Kaçal, H.O. Tekin, Investigation of photon shielding performances of some selected alloys by experimental data, theoretical and MCNPX code in the energy range of 81 keV–1333 keV, J. Alloys Compd. 772 (2019) 516–524, https://doi.org/10.1016/j.jallcom.2018.09.177.

[9] B. Aygün, High alloyed new stainless steel shielding material for gamma and fast neutron radiation, Nucl. Eng. Technol. 52 (3) (2020) 647–653, https://doi.org/10.1016/j.net.2019.08.017.

[10] Y. Al-Hadeethi, M. Ahmed, S.H. Al-Heniti, M.I. Sayyed, Y.S. Rammah, Rare earth Co-Doped tellurite glass ceramics: potential use in optical and radiation shielding applications, Ceram. Int. 46 (11) (2020) 19198–19208, https://doi.org/10.1016/j.ceramint.2020.04.257.

[11] E. Kavaz, F.I. El-Agawany, H.O. Tekin, U. Perişanoğlu, Y.S. Rammah, Nuclear radiation shielding using barium borosilicate glass ceramics, J. Phys. Chem. Solid. 142 (March, 2020), https://doi.org/10.1016/j.jpcs.2020.109437.

[12] Y. Al-Hadeethi, M.I. Sayyed, X-ray attenuation features of some tellurite glasses evaluated at medical diagnostic energies, Appl. Math. Comput. 365 (2020), 124712, https://doi.org/10.1016/j.amc.2019.124712.

[13] R. Bagheri, A. Khorrami Moghaddam, H. Yousefnia, Gamma ray shielding study of barium–bismuth–borosilicate glasses as transparent shielding materials using MCNP-4C code, XCOM program, and available experimental data, Nucl. Eng. Technol. 49 (1) (2017) 216–223, https://doi.org/10.1016/j.net.2016.08.013.

[14] H.O. Tekin, L.R.P. Kassab, O. Kilicoglu, E.S. Magalhães, S.A.M. Issa, G.R. da Silva Mattos, Newly developed tellurium oxide glasses for nuclear shielding applications: an extended investigation, J. Non-Cryst. Solids 528 (2020), 119763, https://doi.org/10.1016/j.jnoncrysol.2019.119763. October 2019.

[15] T.A. Almeida Junior, M.S. Nogueira, V. Vivolo, M.P.A. Potiens, L.L. Campos, Mass attenuation coefficients of X-rays in different barite concrete used in radiation protection as shielding against ionizing radiation, Radiat. Phys. Chem. 140 (2017) 349–354, https://doi.org/10.1016/j.radphyschem.2017.02.054. February.

[16] H.S. Alorfi, M.A. Hussein, S.A. Tijani, The use of rocks in lieu of bricks and concrete as radiation shielding barriers at low gamma and nuclear medicine energies, Construct. Build. Mater. 251 (2020), 118908, https://doi.org/10.1016/j.conbuildmat.2020.118908.

[17] B. Aygün, O. Agar, M.I. Sayyed, A. Karabulut, V.P. Singh, Progress in Nuclear Energy Development of new heavy concretes containing chrome-ore for nuclear radiation shielding applications, Prog. Nucl. Energy 133 (2021), https://doi.org/10.1016/j.pnucene.2021.103645. December 2020.

[18] N.J. AbuAlRoos, N.A. Baharul Amin, R. Zainon, Conventional and new lead-free radiation shielding materials for radiation protection in nuclear medicine: a review, Radiat. Phys. Chem. 165 (August, 2019), https://doi.org/10.1016/j.radphyschem.2019.108439.

[19] Y. Al-Hadeethi, S.A. Tijani, The use of lead-free transparent 50BaO-(50-x)borosilicate-xBi2O3 glass system as radiation shields in nuclear medicine, J. Alloys Compd. 803 (2019) 625–630, https://doi.org/10.1016/j.jallcom.2019.06.259.

[20] C.V. More, H. Alavian, P.P. Pawar, Evaluation of gamma-ray attenuation characteristics of some thermoplastic polymers: experimental, WinXCom and MCNPX studies, J. Non-Cryst. Solids 546 (2020), 120277, https://doi.org/10.1016/j.jnoncrysol.2020.120277. July.

[21] E. Kavaz, H.O. Tekin, G. Kilic, G. Susoy, Newly developed Zinc-Tellurite glass system: an experimental investigation on impact of Ta2O5 on nuclear radiation shielding ability, J. Non-Cryst. Solids 544 (2020), 120169, https://doi.org/10.1016/j.jnoncrysol.2020.120169. June.

[22] S. Yasmin, et al., The radiation shielding offered by the commercial glass installed in Bangladeshi dwellings, Radiat. Eff. Defect Solid 173 (7–8) (2018) 657–672, https://doi.org/10.1080/10420150.2018.1493481.

[23] S. Yasmin, et al., Studies of ionizing radiation shielding effectiveness of silica-based commercial glasses used in Bangladeshi dwellings, Results Phys. 9 (2018) 541–549, https://doi.org/10.1016/j.rinp.2018.02.075.

[24] G. Lakshminarayana, et al., TeO2–B2O3–ZnO–La2O3 glasses: γ-ray and neutron attenuation characteristics analysis by WinXCOM program, MCNP5, Geant4, and Penelope simulation codes, Ceram. Int. 46 (10) (2020) 16620–16635, https://doi.org/10.1016/j.ceramint.2020.03.235.

[25] K. Boonin, et al., Effect of BaO on lead free zinc barium tellurite glass for radiation shielding materials in nuclear application, J. Non-Cryst. Solids 550 (May) (2020), 120386, https://doi.org/10.1016/j.jnoncrysol.2020.120386.

[26] M. Dong, et al., The potential use of boron containing resources for protection against nuclear radiation, Radiat. Phys. Chem. 188 (2021), 109601, https://doi.org/10.1016/j.radphyschem.2021.109601. April.

[27] M.I. Sayyed, H. Akyildirim, M.S. Al-Buriahi, E. Lacomme, R. Ayad, G. Bonvicini, Oxyfluoro-tellurite-zinc glasses and the nuclear-shielding ability under the substitution of AlF3 by ZnO, Appl. Phys. Mater. Sci. Process 126 (2) (2020) 1–12, https://doi.org/10.1007/s00339-019-3265-6.

[28] E. Kavaz, N. Ekinci, H.O. Tekin, M.I. Sayyed, B. Aygün, U. Perişanoğlu, Estimation of gamma radiation shielding qualification of newly developed glasses by using WinXCOM and MCNPX code, Prog. Nucl. Energy 115 (2019) 12–20, https://doi.org/10.1016/j.pnucene.2019.03.029. February.

[29] D.A. Brown, et al., ENDF/B-VIII.0: the 8th major release of the nuclear reaction data library with CIELO-project cross sections, new standards and thermal

scattering data, Nucl. Data Sheets 148 (2018), https://doi.org/10.1016/j.nds.2018.02.001, 1–142.
[30] D.E. Cullen, A Survey of Photon Cross Section Data for Use in EPICS2017, IAEA-NDS-225, rev.1, 2018.
[31] F.C. Hila, A.V. Amorsolo, A.M.V. Javier-Hila, N.R.D. Guillermo, A simple spreadsheet program for calculating mass attenuation coefficients and shielding parameters based on EPICS2017 and EPDL97 photoatomic libraries, Radiat. Phys. Chem. 177 (2020), 109122, https://doi.org/10.1016/j.radphyschem.2020.109122. July.
[32] M.I. Sayyed, et al., Radiation shielding characteristics of selected ceramics using the EPICS2017 library, Ceram. Int. (2021), https://doi.org/10.1016/j.ceramint.2021.01.183.
[33] F. C. Hila, M. I. Sayyed, A. M. V. Javier-Hila, and J. F. M. Jecong, "Evaluation of the radiation shielding characteristics of several glass systems using the EPICS2017 library," Arabian J. Sci. Eng., vol. 47, no. 1, pp. 1077–1086, Jan. 2022, doi: 10.1007/s13369-021-06062-z.
[34] A.H. Almuqrin, J.F.M. Jecong, F.C. Hila, C.V. Balderas, M.I. Sayyed, Radiation shielding properties of selected alloys using EPICS2017 data library, Prog. Nucl. Energy 137 (Jul. 2021), 103748, https://doi.org/10.1016/j.pnucene.2021.103748.
[35] F.C. Hila, et al., Evaluation of photon radiation attenuation and buildup factors for energy absorption and exposure in some soils using EPICS2017 library, Nucl. Eng. Technol. 53 (11) (2021) 3808–3815, https://doi.org/10.1016/j.net.2021.05.030.
[36] F.C. Hila, et al., EpiXS: a Windows-based program for photon attenuation, dosimetry and shielding based on EPICS2017 (ENDF/B-VIII) and EPDL97 (ENDF/B-VI.8), Radiat. Phys. Chem. 182 (May 2021), 109331, https://doi.org/10.1016/j.radphyschem.2020.109331. January.
[37] N. Jamal AbuAlRoos, M.N. Azman, N.A. Baharul Amin, R. Zainon, Tungsten-based material as promising new lead-free gamma radiation shielding material in nuclear medicine, Phys. Med. 78 (2020) 48–57, https://doi.org/10.1016/j.ejmp.2020.08.017. August.
[38] F. Akman, et al., Shielding features, to non-ionizing and ionizing photons, of FeCr-based composites, Appl. Radiat. Isot. 167 (2021), 109470, https://doi.org/10.1016/j.apradiso.2020.109470. August 2020.
[39] S.S. Obaid, D.K. Gaikwad, P.P. Pawar, Determination of gamma ray shielding parameters of rocks and concrete, Radiat. Phys. Chem. 144 (2018) 356–360, https://doi.org/10.1016/j.radphyschem.2017.09.022. September 2017.